Debond Localization in Honeycomb Core Sandwich Composites Using A0 Guided Wave Mode

AUROVINDA KUMAR MITRA and DHANASHRI M. JOGLEKAR

ABSTRACT

Honeycomb core composite sandwich structures (HCCSSs) are widely employed in the marine, defense, and aerospace industries due to their lightweight design, the superior ratio of strength-to-weight and high load-bearing capabilities. Regardless of such commendable advantages, the skin-core junctions are susceptible to debond damage from intensive loading on these structures that may threaten the safety and structural integrity of the assembly. In this study, a novel framework for the guided wave based non-destructive evaluation (NDE) of a three-dimensional HCCSS is presented. The total focusing method with full matrix capture (TFM-FMC) technique is employed to detect and quantify debond at multiple locations in the finite element model of the three-dimensional HCCSS. The fundamental antisymmetric (A0) mode of guided waves is considered for multiple debond assessments in the investigated structure. The A-scan responses of the propagating guided wave of a debond HCCSS are compared with that of a pristine model. This comparison served as a valuable damage precursor resulting from interaction effects. A substantial amplification of the modal amplitude in the case of debonded HCCSS is noticed compared to that of the pristine model. The A-scan responses captured at a location distant from the debonded zone showed little difference. The TFM-FMC algorithm based structural monitoring framework is utilized to locate and quantify the debonded zones in the HCCSS. The proposed health monitoring framework is considered to be substantially effective in the detection of debond damages in a composite sandwich structure.

INTRODUCTION

Composite sandwich structures, composed of a honeycomb core sandwiched between a couple of face sheets, have gained widespread recognition in the aerospace, marine, and automotive industries. This is primarily due to their attractive features,

Aurovinda Kumar Mitra, PhD Student, Email: aurovinda_m@me.iitr.ac.in. Department of Mechanical and Industrial Engineering, Indian Institute of Technology Roorkee 247667, India.
Dhanashri M. Joglekar, Assistant Professor, Email: dhanashri.joglekar@me.iitr.ac.in. Department of Mechanical and Industrial Engineering, Indian Institute of Technology Roorkee 247667, India.

which encompass a high strength-to-weight ratio, lightweight configuration, and exceptional load-bearing capacity [1,2]. Despite their advantages, honeycomb core composite sandwich structures (HCCSSs) are susceptible to debonding damage at the core-skin interface, particularly under intense or repeated dynamic loading on the honeycomb core, due to the bonding interface's weak shear strength [3]. This debonding damage is not apparent to the naked eye, occurring internally between the face sheets and the honeycomb core. However, identifying and quantifying such concealed damage is essential as it significantly affects the structure's integrity.

Guided wave (GW) based non-destructive evaluation (NDE) of various structures have attracted significant attention in research, as they can detect relatively small damages that cannot be observed through conventional visual inspections [4–6]. Moreover, their propensity to travel long distances without significant loss of amplitude makes them an ideal tool for assessing long objects such as pipes, rods, and rails.

Efficient methods for non-destructive detection, localization, and measurement of damages have been the focus of research in many leading centers worldwide. Wave based NDE has received significant interest, especially in the assessment of plate-like structures [7–9]. Mei and Giurgiutiu [10] carried out a theoretical and experimental investigation into the propagation of GWs in a damped composite plate. They introduced a semi-analytical finite element (SAFE) method that integrated the Kelvin-Voigt damping model to consider the plate's anisotropic damping effects. The experimental findings, recorded through the utilization of a scanning laser Doppler vibrometer (LDV), corroborated well with the predicted waveforms. In a study conducted by Muller et al. [11], Lamb wave signals are employed to experimentally examine an aluminum square plate for the presence of a circular damage. The authors employed a damage detection framework based on the total focusing method with full matrix capture (TFM-FMC) to generate a contour plot of the damage. A glass fiber-reinforced polymer (GFRP) composite plate is nonlinearly interacted using the fundamental antisymmetric (A_0) Lamb wave mode by Gangwar et al. [12] to successfully detect a through-width delamination.

Previous studies have focused on the use of GWs for monitoring the health of plate-like structures, with limited attention given to actual aerospace structures made up of HCCSSs with a constant core thickness. To address this gap, the current study aims to develop a 3D finite element (FE) model of a constant thickness HCCSS in ABAQUS/6.14 to simulate multiple debond defects using the A_0 GW mode. GW signals from a square arrangement of actuator-receiver pairs are processed using a TFM-FMC based damage detection algorithm to characterize the debond defects randomly located within the region of interest. The effectiveness of the proposed damage imaging technique is exemplified by its ability to provide reliable quantitative information about the debond defects.

NUMERICAL MODELING

In order to enhance accuracy when investigating a complex structural geometry that includes a debond, the ABAQUS/6.14 FE code is utilized instead of analytical methods. The FE model of constant thickness HCCSS includes top and bottom face sheets with a length and width of 400 mm and 160 mm, respectively. The face sheets consist of a four-

layer [0/90/90/0] GFRP composite with a thickness of 0.5 mm, while the honeycomb core comprises 6061 Aluminum alloy and features an 8 mm cell size and a 0.1 mm wall thickness. The maximum overall thickness of the HCCSS is 25 mm. The FE model of the constant thickness HCCSS is depicted in Figure 1 (left subplot). The material properties of the core are specified in Table I, whereas Table II details the material properties of the face sheets, which are obtained according to ASTM standards [13]. It is worth noting that the Young's modulus (E) and shear modulus (G) are expressed in GPa, while the density (ρ) is measured in kg/m^3. Rayleigh damping, with damping coefficients of α = 8x10^3 and β = 5x10^{-10}, is taken into consideration to prevent wave reflections within HCCSS [2].

Recent studies [14,15] have demonstrated that utilizing an excitation frequency within the range of 15-50 kHz can result in the propagation of global guided waves (standing wave patterns) throughout the entire thickness of a structure, enabling the detection of defects regardless of their location within the structure. For the current investigation, a Hann-windowed, five-cycle sinusoidal pulse with a frequency of 25 kHz and a duration of 1.6 milliseconds is utilized as the excitation signal, as represented in Figure 1 (right subplot). A series of radially distributed concentrated loads [16] are applied to 25 mm by 8 mm areas to model the GW actuator. To excite only the A_0 mode, a point-force type actuation is employed in the opposite direction on rectangular regions created on both the top and bottom face sheets. The top and bottom face sheets are linked to the thick core through surface-based tie constraints. Debond zones with areas of 8 sq. mm (represented as Debond:1) and 5 sq. mm (represented as Debond:2) are introduced within the structure at random locations by removing the ties between the core and face sheet, as

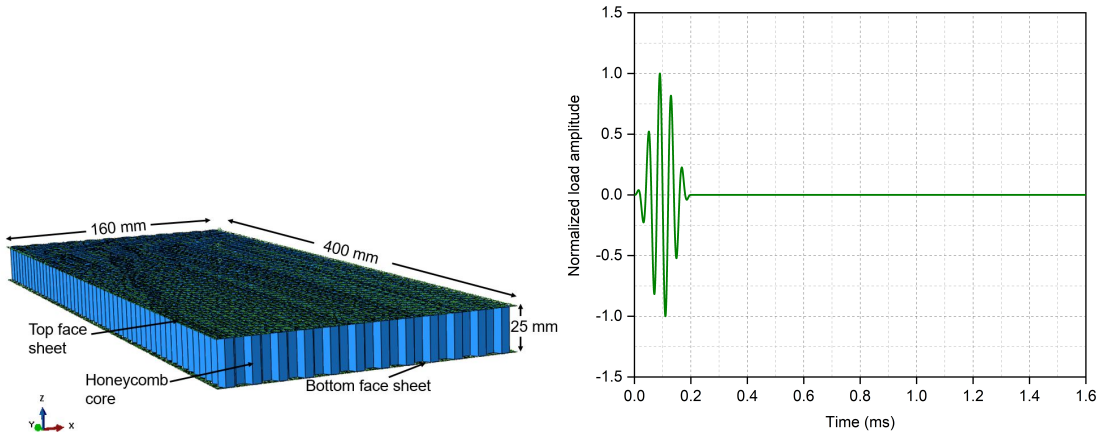

Figure 1. (left) FE model of the constant thickness HCCSS and (right) 25 kHz GW actuation signal.

TABLE I. MATERIAL PROPERTIES OF THE HONEYCOMB CORE.

Material	E	ν	ρ
6061 Al. alloy	69	0.33	2700

TABLE II. MATERIAL PROPERTIES ASSOCIATED WITH THE FACE SHEETS.

Material	E_{11}	E_{22}	E_{33}	G_{12}	G_{13}	G_{23}	ν_{12}	ν_{13}	ν_{23}	ρ
GFRP	44.68	6.9	6.9	2.54	2.54	2.5461	0.28	0.28	0.355	1870

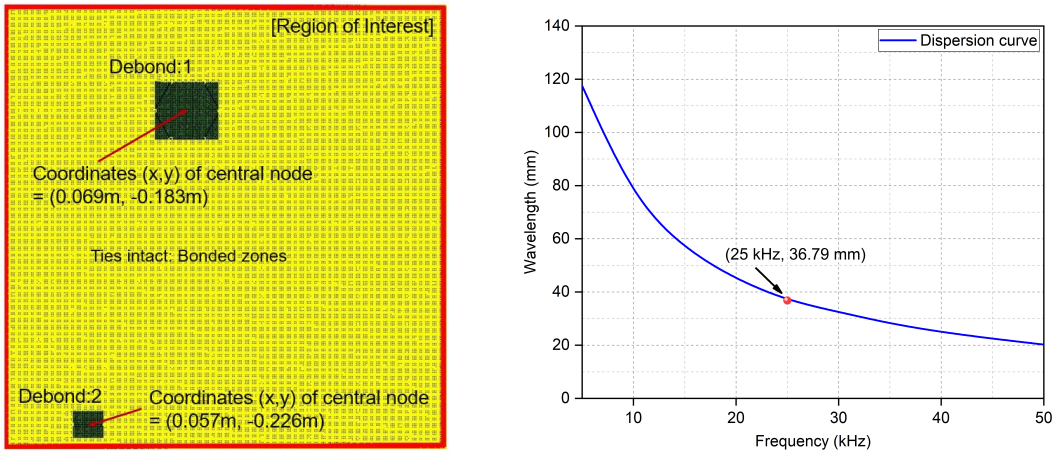

Figure 2. (left) Numerically modeled bonded and debonded zones and (right) wavelength dispersion curve.

evident from Figure 2 (left subplot).

In order to ensure that there are twenty nodes per wavelength, it is essential to adopt an element size that satisfies the required spatial resolution, which can be determined using the following equation:

$$L_e = \frac{\lambda_{\min}}{20}, \tag{1}$$

where L_e represents the mesh size and $\lambda_{\min}$ denotes the smallest wavelength of the propagating wave. A dispersion curve is required within a specific frequency range to determine the minimum wavelength. The SAFE approach is employed for this purpose, which accounts for the core's equivalent homogeneous properties [17]. The dispersion curve represented in Figure 2 (right subplot) shows that the minimum wavelength corresponding to the 25 kHz actuation frequency is 36.79 mm. Therefore, the HCCSS numerical model is discretized using a mesh size of 0.25 mm, ensuring the presence of twenty nodes per wavelength as per Equation 1. In order to model the face sheets and core, the S4R shell element is employed with six degrees of freedom per node.

The selection of the step time (Δt) in the numerical simulation takes two factors into consideration. One factor to consider is ensuring that the sampling frequency, which is the inverse of the Δt, is sufficiently high to accurately capture the wave pattern. This necessitates a minimum sampling frequency that is twenty times higher than the highest frequency employed in the numerical analysis. If $f_{\max}$ represent the maximum excitation frequency, then:

$$\Delta t \leq \frac{1}{(20 f_{\max})}. \tag{2}$$

Secondly, the Δt must fulfill the Courant-Friedrichs-Lewy (CFL) condition [18], which can be stated as follows:

$$\Delta t \leq \frac{L_{min}}{C_{max}}, \tag{3}$$

where L_{min} denotes the smallest distance between two nodes and C_{max} stands for the greatest wave speed. In order to meet both of these criteria, a step time of $1e-8$ s is utilized in the simulations.

The A-scan responses obtained from numerical simulations are processed using the TFM-FMC algorithm, which will be discussed in the upcoming section, to create a contour image of the debonded zones.

THE TFM-FMC DAMAGE IMAGING TECHNIQUE

The TFM is an imaging system for detecting defects that involves an array of transducers located at different positions. In this procedure, the time required for each signal to reach a particular pixel is computed and compared. The FMC relates to the exchanging of positions between transmitting and receiving transducers in a sequential manner [11]. By selecting a group of eight rectangular areas, each measuring 25 mm by 8 mm, and using them in succession as both an actuator and a receiver, a total of 56 wave signals are collected. The placement of actuator and sensors in arbitrary positions is taken into account by:

$$PI_{(x,y)} = \left| \sum_{i=1}^{N} \sum_{j=1}^{N} h_{A_i,R_j}\left(\frac{\sqrt{(x_{A_i}-x)^2+(y_{A_i}-y)^2}+\sqrt{(x_{R_j}-x)^2+(y_{R_j}-y)^2}}{C_G}\right)\right|, \tag{4}$$

in which, $PI_{(x,y)}$ is the pixel intensity situated at the Cartesian coordinates (x, y), h_{A_i,R_j} is the signal envelope acquired from the actuator A_i and the receiver R_j, x_{A_i} and y_{A_i} are the Cartesian coordinates of the actuator A_i, x_{R_j} and y_{R_j} represents the Cartesian coordinates of the sensor R_j, N denotes the total number of actuators and sensors while the C_G is the group velocity of the propagating GW.

The arbitrary positioning of the actuator and sensor is accomplished by computing the distance between each actuator/sensor pair and a particular pixel point in Cartesian coordinates. The calculated group speed is used thereafter to convert the distance into travel time. The amplitude of the signal's envelope associated with this travel time (relative to the actuator/sensor pair) is obtained and incorporated into the intensity of pixel. This process is iteratively performed for each pair of actuators and sensors. The TFM-FMC technique to localize the debond zones is implemented on a region of interest (manifested in Figure 2 (left subplot)) measuring 60 mm by 60 mm area, and all the calculations required for generating the debond image are performed using MATLAB.

RESULTS AND DISCUSSION

Wavefield Images

The out-of-plane wavefield images from the numerical simulations are generated, and a comparison between the wavefield images of a pristine HCCSS and a debonded HCCSS is illustrated in Figure 3. It is observed that the occurrence of debonded zones

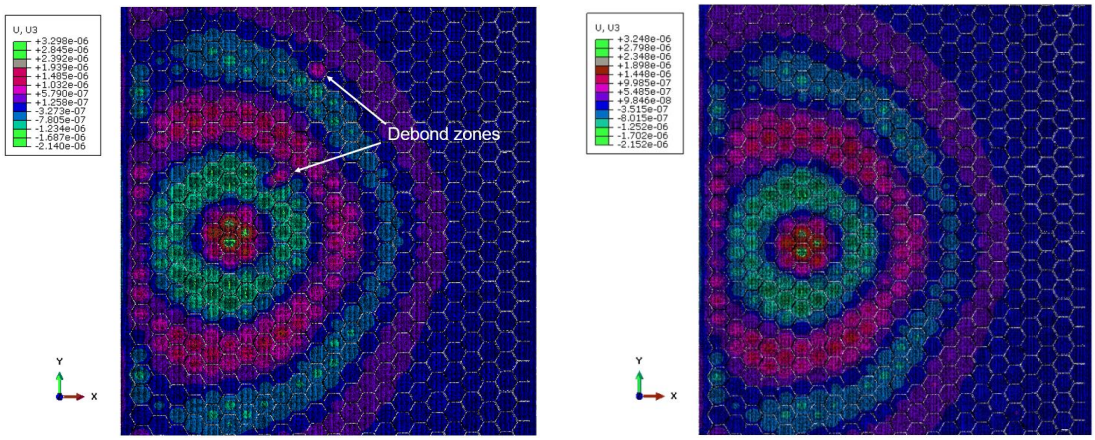

Figure 3. (left) The out-of-plane wavefield image of the debonded HCCSS and (right) pristine HCCSS.

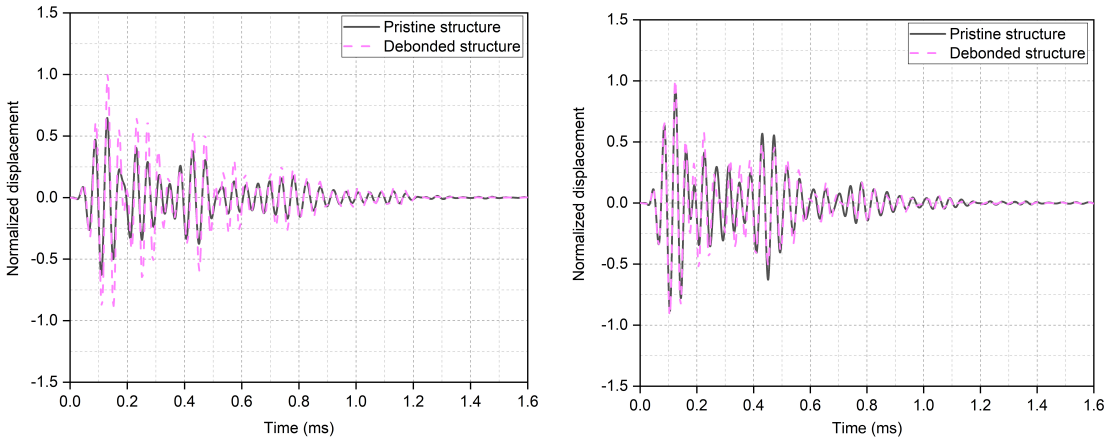

Figure 4. (left) Comparison of the A-scan responses at the center of the debonded zone and (right) at a location distant from the debonded zone.

resulted in the interruption of wave propagation in the debonded HCCSS. In contrast to the debonded HCCSS, waves propagated smoothly without any interruptions in the pristine HCCSS (shown in Figure 3(right subplot)). Moreover, the waves propagating through the debonded zones exhibited higher strengths compared to the waves propagating in the pristine condition.

Debond Effect

To analyze the influence of debonding on wave propagation mode, the output signals of the HCCSS are compared at two different locations: before the debonded region and at the center of the debonding. These signals are then compared with the signals obtained from the pristine HCCSS. The comparison results are displayed in Figure 4. The results indicated that the presence of the debond region substantially amplified the propagating A_0 mode in the received signals (Figure 4(left subplot)). Nonetheless, little difference is observed in the A-scan responses captured at a location distant from the debonded zone (Figure 4(right subplot)).

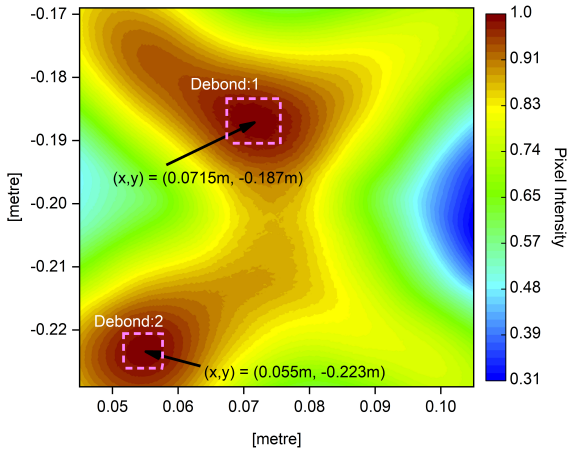

Figure 5. The contour image of the debonded zones acquired using the TFM-FMC technique.

Localization of the Debonded Zones in HCCSS

The group speed of the propagating GWs, determined using the cross-correlation technique [19], is calculated to be 953.62 m/s. This value is then integrated into the TFM-FMC algorithm based structural monitoring framework to accurately locate and quantify the debonded zones in the HCCSS. The predicted debond zones, identified based on the higher pixel intensities observed in the TFM-FMC map shown in Figure 5, demonstrated good correlation with the actual debond areas (Figure 2 (left subplot)).

CONCLUDING REMARKS

The propagation of the A_0 GW mode in a 3D HCCSS to detect multiple debonds is numerically studied. The wavefield image of the pristine HCCSS showed smooth wave propagation, while the image related to the debonded HCCSS displayed a marked interruption in the wavefield patterns. The amplitude of the A_0 mode experienced a significant enhancement in the presence of debonded regions, whereas little differences are observed in the A-scan responses obtained at a location distant from the debonded zone. The TFM-FMC structural monitoring algorithm is utilized for detecting and quantifying the debond regions in the HCCSS. The algorithm's ability to detect debond regions within the actuator/sensor array suggests its potential for large-scale non-destructive inspections of HCCSS using the GW technique.

REFERENCES

1. Yoon, S., A. Schiffer, W. J. Cantwell, and T.-Y. Kim. 2021. "Detection of core-skin disbonds in honeycomb composite sandwich structures using highly nonlinear solitary waves," *Composite Structures*, 256:113071.
2. Mitra, A. K., A. A. Aradhye, and D. M. Joglekar. 2023. "Low frequency ultrasonic guided wave propagation through honeycomb sandwich structures with non-uniform core thickness," *Mechanical Systems and Signal Processing*, 191:110155.

3. Song, F., G. Huang, and G. Hu. 2012. “Online guided wave-based debonding detection in honeycomb sandwich structures,” *AIAA Journal*, 50(2):284–293.
4. Su, Z., L. Ye, and Y. Lu. 2006. “Guided Lamb waves for identification of damage in composite structures: A review,” *Journal of sound and vibration*, 295(3-5):753–780.
5. Raghavan, A. and C. E. Cesnik. 2008. “Effects of elevated temperature on guided-wave structural health monitoring,” *Journal of Intelligent Material Systems and Structures*, 19(12):1383–1398.
6. Wu, Y., K. Zhang, C. L. Huang, S. Lee, J. Popovics, and X. Zhu. 2021. “On the Existence of Zero Group Velocity Modes in Rails,” in *13th International Workshop on Structural Health Monitoring: Enabling Next-Generation SHM for Cyber-Physical Systems, IWSHM 2021*, DEStech Publications Inc., pp. 695–702.
7. Gangwar, A. S., Y. Agrawal, and D. Joglekar. 2021. “Nonlinear interactions of Lamb waves with a delamination in composite laminates,” *Journal of Nondestructive Evaluation, Diagnostics and Prognostics of Engineering Systems*, 4(3).
8. Radzieński, M., Ł. Doliński, M. Krawczuk, and M. Palacz. 2013. “Damage localisation in a stiffened plate structure using a propagating wave,” *Mechanical Systems and Signal Processing*, 39(1-2):388–395.
9. Gangwar, A. G. and D. M. J. Joglekar. 2022. “Investigation of higher harmonic Lamb waves for facilitating delamination characterization,” in *ECCOMAS Congress 2022-8th European Congress on Computational Methods in Applied Sciences and Engineering*.
10. Mei, H. and V. Giurgiutiu. 2019. “Guided wave excitation and propagation in damped composite plates,” *Structural Health Monitoring*, 18(3):690–714.
11. Muller, A., B. Robertson-Welsh, P. Gaydecki, M. Gresil, and C. Soutis. 2017. “Structural health monitoring using Lamb wave reflections and total focusing method for image reconstruction,” *Applied Composite Materials*, 24:553–573.
12. Gangwar, A. S., Y. Agrawal, and D. M. Joglekar. 2022. “Effects of Delamination on Higher Harmonics Generation in Unidirectional GFRP Laminate,” in *Advances in Non Destructive Evaluation: Proceedings of NDE 2020*, Springer, pp. 411–421.
13. Agrawal, Y., A. S. Gangwar, and D. Joglekar. 2022. “Localization of a breathing delamination using nonlinear lamb wave mixing,” *Journal of Nondestructive Evaluation, Diagnostics and Prognostics of Engineering Systems*, 5(3):031005.
14. Yu, L., Z. Tian, X. Li, R. Zhu, and G. Huang. 2019. “Core–skin debonding detection in honeycomb sandwich structures through guided wave wavefield analysis,” *Journal of Intelligent Material Systems and Structures*, 30(9):1306–1317.
15. Song, F., G. Huang, and K. Hudson. 2009. “Guided wave propagation in honeycomb sandwich structures using a piezoelectric actuator/sensor system,” *Smart Materials and Structures*, 18(12):125007.
16. Mustapha, S. and L. Ye. 2015. “Propagation behaviour of guided waves in tapered sandwich structures and debonding identification using time reversal,” *Wave Motion*, 57:154–170.
17. Vinson, J. R. and R. L. Sierakowski. 2006. *The behavior of structures composed of composite materials*, vol. 105, Springer.
18. Agrawal, Y., A. S. Gangwar, and D. M. Joglekar. 2022. “Effect of Ply Orientation on Nonlinear Lamb Wave Delamination Interactions in GFRP Composite Laminates,” in *Advances in Non Destructive Evaluation: Proceedings of NDE 2020*, Springer, pp. 423–434.
19. Hernandez Crespo, B., C. R. Courtney, and B. Engineer. 2018. “Calculation of guided wave dispersion characteristics using a three-transducer measurement system,” *Applied sciences*, 8(8):1253.